Analyst

Cite this: *Analyst*, 2011, **136**, 1210

www.rsc.org/analyst

PAPER

Development of double cylindrical dielectric barrier discharge ion source

Kenzo Hiraoka,*[a] Satoshi Ninomiya,[b] Lee Chuin Chen,[b] Takashi Iwama,[c] Mridul Kanti Mandal,[a] Hiroaki Suzuki,[d] Osamu Ariyada,[d] Hiroko Furuya[e] and Kenichi Takekawa[e]

Received 10th August 2010, Accepted 20th December 2010
DOI: 10.1039/c0an00621a

This paper deals with the dielectric barrier discharge (DBD) ion source composed of the outer cylindrical dielectric tube and the inner grounded metallic tube electrode. The sample gas is supplied through the inner ceramic tube. In this ion source, the DBD plasma is localized in the DBD tube so that the sample gases can be ionized just outside of the ceramic tube by the DBD excited helium gas without being exposed in the plasma jet. Besides, ambient air does not take part in the ionization of the sample vapor because ionization takes place inside the DBD ion source. Thus, this method is totally free from contaminants in ambient air. It was found that this ion source is capable of soft, high-sensitivity, and reproducible ionization. Application of this technique to the analysis of methamphetamine, carbaryl and basil leaf was given.

Introduction

The direct-current (DC) corona discharge has been used for the atmospheric-pressure chemical ionization (APCI) for a long time period since its introduction by Horning *et al.* for the analysis of volatile compounds.[1]

Since then, various types of ion sources have been developed by means of DC corona discharge. Cody *et al.* developed a new ion source using DC corona discharge for the analysis of materials in open air under ambient conditions. This technique was applied to the direct sampling and ionization of pharmaceuticals, metabolites, peptides, oligosaccharides, synthetic organics, organometallics, drugs of abuse, explosives and toxic industrial chemicals as direct analysis in real time (DART).[2] The limit of detection (LOD) was found to be ~2 pg for ethyl palmitate deposited on a glass rod using a time-of-flight mass spectrometer.

Chen *et al.* developed a DC corona discharge ionization source adapted for direct surface desorption atmospheric pressure chemical ionization (DAPCI) of compounds on various surfaces using an ion trap mass spectrometer.[3] Ambient air, with about 60% relative humidity, is used as a reagent of the discharge to generate primary ions such as H_3O^+. In DAPCI, the DC corona discharge was directly exposed to the sample surface for desorption and ionization. This method provided an LOD in the sub-picogram range (S/N ≥3) in MS^2 using an ion trap mass spectrometer.

In addition to the DC corona discharge ion source, dielectric barrier discharge (DBD) has recently been developed as the ionization source for mass spectrometry.[4–12] DBD can generate plasma with plasma densities two to three orders of magnitude higher than the DC corona discharge, *i.e.*, *ca.* 10^{12}–10^{15} cm^{-3}.[13] To exploit this merit, Zhang and co-workers first developed the ion source using DBD in 2007.[4,5] Due to its high plasma density, abundant ionizing reagents (*e.g.*, electronically excited metastable species, positive and negative reagent ions and electrons) should be generated by the DBD ion source.[13] This work triggered the application of DBD to mass spectrometry.[7,9] In these works, the sample surfaces were exposed by the DBD plasma jet. The main aim for the exposure of the plasma jet on the sample surface is to promote desorption of the analyte molecules from the surface followed by ionization of the desorbed molecules by the DBD plasma. By using a DBD ion source, Harper *et al.* demonstrated that explosives such as RDX (hexahydro-1,3,5-trinitro-1,3,5-triazine) and TNT (2,4,6-trinitrotoluene) from a PTFE (poly(tetrafluoroethylene)) surface could be detected with an LOD as low as 5 pg by tandem mass spectrometry.[7]

Although the method of exposing the plasma directly to the sample surface is a versatile method for ambient ionization mass spectrometry, the formation of fragment ions is inevitable because ionization takes place in plasma in which energetic electrons are present. In addition, some plasma-induced products were also formed due to the complicated secondary reactions taking place in the plasma. For example, Na *et al.* found that almost all benzene molecules introduced into the helium DBD plasma were hydrogenated to cyclohexadiene *etc.*, *i.e.*, the occurrence of Birch reduction of benzene in the low temperature plasma.[8]

[a]*Clean Energy Research Center, University of Yamanashi, 4-3-11 Takeda, Kofu, Yamanashi, 400-8511, Japan. E-mail: hiraoka@yamanashi.ac.jp; Fax: +81 552208709; Tel: +81 552208572*
[b]*Interdisciplinary Graduate School of Medical and Engineering, University of Yamanashi, 4-3-11 Takeda, Kofu, Yamanashi, Japan*
[c]*The Yamanashi Prefectural Industrial Technology Center, 2094, Ootsumachi, Kofu, Yamanashi, Japan*
[d]*ARIOS INC. Akishima, Tokyo, Japan*
[e]*Forensic Science Laboratory, Yamanashi Prefectural Police H.Q., Fuefukishi, Yamanashi, Japan*

We were also investigating the application of DBD to mass spectrometry at about the same time of Zhang's pioneering work.[4,5] At that time, the main objective of our research was focused on the detection of explosives such as DNT (dinitrotoluene), TNT, TATP (triacetone triperoxide), HMTD (hexamethylene triperoxide diamine), *etc.* for the governmental security/safety project (Collaborative Development of Innovative Seeds, 'Science & Technology Project for a Safe & Secure Society', Japan and Science Technology Agency, 2007–2008). In our preliminary experiment, we used a discharge tube that consisted of a cylindrical quartz tube (*i.e.*, dielectric) with an inner diameter of 4 mm. The electrodes consisted of a stainless steel wire (inner electrode) and a copper strip (outer electrode). This system was similar to the one adopted by Harper *et al.*[7] In this configuration, the inner electrode was recessed inside the quartz tube. By the application of an AC voltage between the two metal electrodes, an extended DBD plasma jet was formed outside the quartz tube. We tried to desorb/ionize the explosive samples by exposing them to the DBD plasma jet in ambient air. It was found that the fragment ions and also ions whose *m*/*z* values were higher than the molecular weights of analytes were produced, although protonated molecules and/or molecular ions were detected with reasonable abundances. The formation of higher-mass ions was a serious problem in our research project, because it would give the false-positive ion signals in the safety/security applications. It was found that the relative abundances of fragment ions and higher-mass ions to those of the protonated molecules and molecular ions decreased drastically when the distance between the plasma and the sample was increased. Therefore, the fragment ions and higher-mass ions must have mainly originated from some complex chemical reactions taking place in the DBD plasma in which energetic electrons should play a major role. Due to this drawback, we have withdrawn the idea of exposing the sample in the plasma jet.

After some trial and error, we have develop a new DBD ion source that can cut off the plasma jet coming out from the exit of the quartz tube. This new type of DBD ion source has almost the same configuration as the former one. The only difference is that the tip of the grounded inner wire electrode is positioned near the exit of the quartz tube or even extended slightly outside of the quartz tube.[10–12] This small modification made it possible to confine the DBD plasma inside the quartz discharge tube resulting in the increase in the molecular ion signal intensities with the ability of soft ionization for various gaseous sample molecules. This ion source was found to be versatile for the detection of not only explosives but also vapor samples.[10–12] However, we found that the ion signal intensities often fluctuated depending on the sample position introduced between the DBD ion source and the ion sampling orifice. Besides, contaminants present in the ambient air always appeared as the background signals (*e.g.*, $[(H_2O)_n + H]^+$, $[\text{acetone} + H]^+$, *etc.*).

In order to eliminate this drawback inherent to the open-air ambient DBD discharge developed in our laboratory, the non-ambient DBD ion source was newly developed in this work. This new type of ion source was found to be free from contamination originating from the ambient air. Another merit of this ion source is its high reproducibility in operation.

Experimental

The conceptual idea of the newly developed DBD ion source is displayed in Fig. 1. To generate the DBD plasma, the sinusoidal signal of 15 kHz generated from a function generator was amplified by a power amplifier and a transformer to several kV to generate an AC high voltage (H.V.). The discharge tube was made of a cylindrical alumina tube (*i.e.*, dielectric) with an inner diameter of 6 mm. The electrodes consist of a copper strip (outer electrode) and a stainless steel tube (inner electrode) with an inner diameter of 3.5 mm inserted to the alumina cylindrical tube. The copper strip electrode was attached on the outer surface of the alumina cylindrical tube. The outer electrode was fed with the AC H.V. with respect to the inner electrode at ground potential. The outer end of the alumina tube was connected with a glass cap. The distance between the terminal end of the glass cap and the ion sampling orifice of the mass spectrometer was 1 mm. The flow rate of He for DBD was $\leq$1 L min^{-1}. The ions generated by the DBD ion source were sampled through the ion sampling orifice and transported to the ion guide for collisional cooling and mass-analyzed by an orthogonal-type time-of-flight mass spectrometer (JEOL, AccuTOF, Akishima, Tokyo, Japan). The ions detected by a microchannel plate were converted to digital signals by a 4 GHz time-to-digital converter.

As shown in Fig. 1, a plastic (polypropylene) vial was put in a plastic sample container (Teflon® PFA). The sample container was pushed up to the upper wall of the sample holder by a screw and sealed tightly to prevent loss of sample vapor. The sample holder has two holes: the inlet and outlet of the N_2 carrier gas (~0.2 L min^{-1}). The N_2 gas carries the sample vapor in the sample container to the alumina ceramic tube. The sample gas was ionized at the terminal end of the alumina tube where the DBD excited He and the N_2 gas containing the sample gas are merged.

In the measurement using the ion source shown in Fig. 1, a plastic vial containing 100 μL of liquid sample was put inside the sample container. Two button heaters were attached to the wall of the sample holder (aluminium block). The temperature was monitored using a thermocouple. After the sample vial was

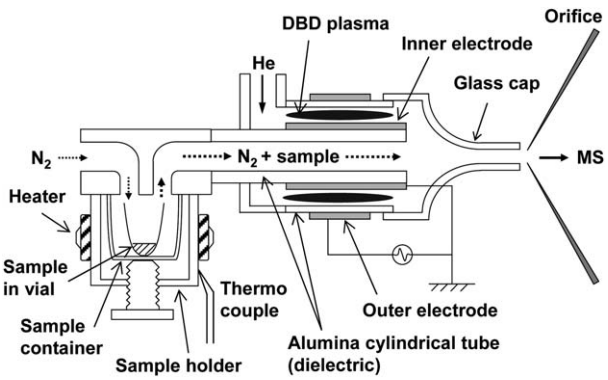

Fig. 1 Structures of the DBD ion source. The DBD plasma is confined in the double cylindrical discharge tube so that the sample gas is not exposed to the DBD He plasma. The sample vial is heated gradually up to 150 °C in about 30 min. Vaporized sample gases are carried by the N_2 gas and transported to the exit of the dielectric tube where the gaseous sample molecules are ionized by the DBD excited He gas.

put inside the sample holder, the button heaters were switched on. The temperature of the sample holder was raised from room temperature to 150 °C in ~2.5 min. Because the thermal contact of the sample vial with the sample holder is not good in this system, the temperature monitored by the thermocouple does not represent that of the sample vial. We roughly estimated that the temperature of the sample vial may reach 150 °C in about 30 min after the button heaters were turned on.

In the DBD ion source shown in Fig. 1, the DBD plasma could be confined in the region of the outer copper sleeve electrode. Thus, the N_2 gas containing sample gas that flows out of the outlet of the ceramic tube is not exposed by the plasma. In such a way the soft ionization of sample molecules is guaranteed by this ion source.

Results and discussion

The novel feature of DBD ion source shown in Fig. 1 is that one of the electrodes is positioned outside the discharge space and is not in contact with the plasma. In their pioneering work, Kanazawa *et al.* found that 'cold' non-equilibrium plasma can be generated at atmospheric pressure by DBD.[14] DBD has the strong influence of the local field distortions caused by space charge accumulation on the dielectric. The dielectric that separates the two electrodes limits the discharge current due to charge accumulation on the dielectric. Thus the initially formed DBD ceases before the transition from glow discharge to arc discharge. In a sense, the dielectric acts as ballast which consumes minimum energy. This explains why the thermal damage of the electrodes and dielectric is largely suppressed in DBD.

In more detail for the DBD ion source in Fig. 1, the wall of the insulator is instantly charged with electrons, because electrons have much higher kinetic energies than ions. In contrast, the positive ions that hit the central tube electrode will escape to the earth, because the central electrode is grounded. Thus, the glow discharge plasma cannot maintain its neutrality but becomes highly negative (*i.e.*, electron-rich), because less-energetic electrons cannot hit the wall but are reflected back in the plasma due to the space charge field generated on the negatively charged wall (*i.e.*, plasma sheath). As such, the plasma potential becomes highly negative with excess electrons. Thus, the high electric field should be generated between the electron-rich plasma and the surrounding earth potential. Due to this high electric field, electrons in the plasma will be accelerated towards the inner ground-potential metal tube electrode (Fig. 1). This is the reason why the DBD plasma can be localized in the region of the outer copper electrode.

In our previous work,[15] a study was made of the atmospheric-pressure Penning ionization (APPeI) of aliphatic hydrocarbons (pentane, hexane, heptane, and octane) with metastable rare gas atoms (Rg*: He*, Ne*, Ar*, and Kr*). In the Rg* APPeI mass spectra for aliphatic hydrocarbons, the relative abundances of fragment ions were found to increase in the order of He* → Ne* → Ar* → Kr* → Xe*. The order is in the opposite direction to the internal energies of the Rg*. That is, He* is the softest reagent metastable atom for the ionization of aliphatic hydrocarbons. By using the DBD ion source using He* as shown in Fig. 1, the soft ionization was also realized for all the vapor samples measured with little formation of fragment and higher-mass ions. The sample vapor may be ionized not only by the Penning ionization but also by APCI. As N_2 is used as a carrier gas, the occurrence of reactions (1)–(7) may be likely under the present experimental conditions.[16,17]

$$He^* + M \rightarrow M^+ + e^- + He \quad \text{(Penning ionization)} \quad (1)$$

$$He^* + N_2 \rightarrow N_2^+ + e^- + He \quad \text{(Penning ionization)} \quad (2)$$

$$N_2^+ + N_2 + N_2\,(3rd\ body) \rightarrow N_4^+ + N_2\,(3rd\ body) \quad \text{(clustering reaction)} \quad (3)$$

$$N_4^+ + M \rightarrow M^+ + 2N_2 \quad \text{(charge transfer reaction)} \quad (4)$$

$$N_4^+ + H_2O \rightarrow H_2O^+ + 2N_2 \quad \text{(charge transfer reaction)} \quad (5)$$

$$H_2O^+ + H_2O \rightarrow H_3O^+ + OH \quad \text{(proton or hydrogen atom transfer reaction)} \quad (6)$$

$$H_3O^+ + M \rightarrow [M + H]^+ + H_2O \quad \text{(proton transfer reaction)} \quad (7)$$

Fig. 2(a) shows the total ion chronogram (TIC) for the sample of 100 μL of methamphetamine (MA, $C_{10}H_{15}N$, MW 149.24) aqueous solution with a concentration of 0.9 μg mL^{-1}. The sample of MA used is in the form of chloride salt. The heater is turned on at 0 min. The TIC starts to increase at ~2 min, reaches the plateau at ~5 min and shows a sudden decrease at ~17.5 min and stays constant after ~18 min. A sudden decrease in TIC at ~17.5 min is likely to be due to the total evaporation of water droplets in the sample vial. This has been confirmed in a separate experiment. That is, the ion signals of $[(H_2O)_3 + H]^+$ (*m/z* 55) showed a sudden decrease at 17.5 min for the pure water of 100 μL. The water vapor acts as the reagent gas and contributes to the APCI for various gaseous components in the sample gas

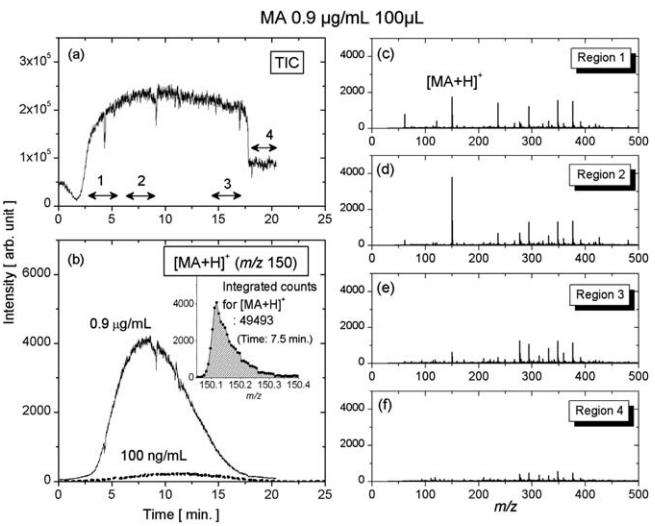

Fig. 2 Experimental results obtained for 0.9 μg mL^{-1} methamphetamine aqueous solution. 100 μL of the sample solution was loaded in a sample vial. (a) Total ion chronogram (TIC); (b) extracted ion chronogram of protonated methamphetamine $[MA + H]^+$ at *m/z* 150, (inset) enlarged peak for $[MA + H]^+$ at *m/z* around 150; (c), (d), (e) and (f) mass spectra measured at the time interval regions of 1, 2, 3, and 4 shown in (a), respectively.

(reaction (7)). The depletion of water droplet in the sample vial results in the decrease of total ion currents due to the decrease of the partial pressure of water vapor.

Fig. 2(b) shows the extracted ion chronogram for protonated methamphetamine $[MA + H]^+$ at *m/z* 150. The ion signal shows a maximum at ~8 min and decreases to nearly zero at 17 min. That is, MA evaporates earlier than water droplets. That is, methamphetamine (MA) in aqueous solution has a higher volatility than liquid water. Because the boiling point of MA (212 °C) is much higher than that of water (100 °C), the preferential evaporation of MA must take place under the present experimental conditions. It is conceivable that the surface of the aqueous solution of MA is highly enriched by hydrophobic (*i.e.*, more surface-active) MA. In the binary components of water and MA, evaporation of MA may become more favorable than water solvent.

Under the present experimental conditions, the ion guide was adjusted to measure the *m/z* region higher than ~50. Therefore, fragment ions with *m/z* below 50 could not be detected if there were any. The ion with *m/z* 61 was detected, but the extended ion chronogram for this ion did not agree with that for *m/z* 150. Thus, the ion with *m/z* 61 should not be the fragment ion originating from MA. The background ions with *m/z* above 200 were not identified.

It should be noted that the extracted ion chronogram shown in Fig. 2(b) just follows the most intense count of the peak around *m/z* 150, given by the software pre-installed in the mass spectrometer control PC used in this measurement. That is, the intensities of $[MA + H]^+$ in Fig. 2(b) correspond to the 'peak' (*i.e.*, maximum) counts in the mass spectra shown in Fig. 2(c)–(f) at each time. The inset in Fig. 2(b) shows the enlarged mass spectrum around *m/z* 150 at 8 min. As shown in the inset, the integrated total counts around *m/z* 150 calculated by hand work were 43 493, and account for 20% of the total ion current in Fig. 2(a) at 8 min. Namely, the intensity of Fig. 2(a) corresponds to the integrated ion counts of all ions in the mass spectrum including noise peaks. This is the reason why the ion counts auto-calculated by the PC software in Fig. 2(a) are much larger than the peak count of each ion signal.

Fig. 2(c)–(f) show the mass spectra measured at the time interval regions of 1, 2, 3 and 4 shown in Fig. 2(a), respectively. The protonated methamphetamine $[MA + H]^+$ is observed as a base peak with little fragment ions in the mass spectra of (c)–(e), indicating that the present DBD ion source realizes the soft ionization. The peaks appearing at *m/z* 61, 121, and 236 are not fragment ions of MA but originate from impurities, because they persisted to appear when no sample was loaded in the sample vials. These peaks could not be identified.

In our previous work using a DBD ion source under ambient conditions,[10–12] almost always the protonated acetone $[(CH_3)_2CO + H]^+$ at *m/z* 59 was observed as one of the major background ion signals due to the contamination of laboratory air by acetone vapor. In Fig. 2(c)–(f), however, no protonated acetone was observed. This is expected because laboratory air does not take part in the ionization in the present DBD ion source (see Fig. 1). Thus, the present ion source is totally free from contaminants in ambient air.

Organic acids and bases (*e.g.*, amines) dissolved in aqueous solution may partly exist as ionic forms. Since ionic forms are much more hydrophilic than neutral forms, the ionic forms must have lower vapor pressures than their neutral forms and thus are less evaporative. The electrolytic dissociation equilibrium of organic acids or bases can be controlled by changing the pH of the aqueous solution. In the case of organic bases such as MA, the addition of stronger bases such as NaOH or ammonia will shift the equilibrium toward the neutral forms. In order to examine the effect of solution pH, the ion intensities for $[M + H]^+$ for the aqueous solution of the chloride salt of MA (1 μg mL^{-1}) with and without the addition of NaOH and aqueous NH_3 were examined.

Fig. 3(a)–(c) and (d)–(f) show the TIC and extracted ion chronograms for $[MA + H]^+$ for three samples [MA 1 μg mL^{-1}: 90 μL + pure H_2O: 10 μL], [MA 1 μg mL^{-1}: 90 μL + 1 N NaOH(aq): 10 μL] and [MA 1 μg mL^{-1}: 90 μL + 28% NH_3(aq): 10 μL], respectively. While the TIC in Fig. 3(a) and (b) are almost identical, the TIC in Fig. 3(c) shows initial steep increase followed by a gradual decrease. Because ammonia is a weak base and much more evaporative than water, the initial steep increase in TIC may be due to the rapid evaporation of NH_3 from the solution followed by the formation of NH_4^+ and NH_4^+-related ions, *e.g.*, cluster ions of NH_4^+ with various impurity molecules. The decrease in TIC and increase in $[MA + H]^+$ at ~3 min in Fig. 3(c) may partly be ascribed to the occurrence of proton transfer reactions to form $[MA + H]^+$, for example, reaction (8).[17]

$$NH_4^+ + MA \rightarrow [MA + H]^+ + NH_3 \quad (8)$$

Actually, ammonia is used as a standard reagent gas for chemical ionization of analytes whose proton affinities are higher than NH_3.[18]

The marked difference between Fig. 3(d) and Fig. 3(e) and (f) is that the onsets of the ion intensities for $[M + H]^+$ for (e) and (f) are much faster than that of (d). In addition, the maxima of the ion intensities in Fig. 3(e) and (f) shift to shorter time (~4.5 min) as compared with Fig. 3(d) (~8 min). It is evident that the evaporation of MA is enhanced considerably by the addition of

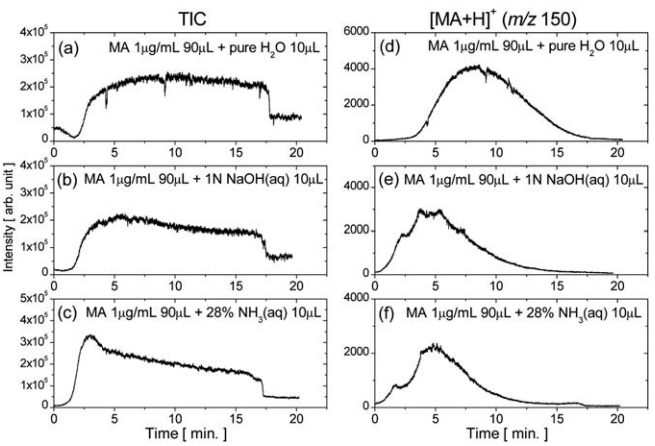

Fig. 3 (a)–(c) TIC for three samples [MA 1 μg mL^{-1}: 90 μL + pure H_2O: 10 μL], [MA 1 μg mL^{-1}: 90 μL + 1 N NaOH(aq): 10 μL], and [MA 1 μg mL^{-1}: 90 μL + 28% NH_3(aq): 10 μL], respectively; (d)~(f) extracted ion chronograms for $[MA + H]^+$ for the three samples. Sample volume loaded: 100 μL.

NaOH and also NH_3 in MA aqueous solution. Since the sample amounts of MA loaded in the measurements for Fig. 3(d)–(f) were the same (90 ng), the time-integrated total ion intensities of Fig. 3(d), (e) and (f) should be the same. However, the time-integrated area of Fig. 3(e) and (f) are apparently smaller than that of Fig. 3(d). This may be due to the evaporative loss of MA during the sample preparation. It took about 2 min for the sample preparation of the addition of NaOH or NH_3 to the aqueous solution of MA and putting the vial into the sample holder. After the sample vial was put into the sample holder, the nitrogen gas was flowed for about 5 min before the mass spectrometric measurements, *i.e.*, start of heating. During this sample preparation, some evaporative loss of MA may take place. The new type of ion source is being developed in our laboratory that makes it possible to make the sample preparation time much shorter.

Fig. 4 shows the calibration curve measured for the quantitative analysis of MA. In this figure, the MA concentration [ng mL^{-1}] and the integrated intensities for $[MA + H]^+$ for [aqueous solution of MA: 90 μL + 1 N NaOH(aq): 10 μL] are plotted. Reasonably good linearity in Fig. 4 suggests that the present method may be applicable to the quantitative analysis of vaporizable ingredients in physiological fluids such as urine. In Fig. 2(b), the extracted ion chronogram for $[MA + H]^+$ for the sample with an MA concentration of 100 ng mL^{-1} (sample amount loaded: 10 ng) was given as a dotted lines. As shown in the figure, the ion was observed for about 10 min with an S/N ratio of about 10. The signal integration time of the digital signal averager was adjusted to be 0.5 s. The sample amount supplied to the ion sampling orifice of the mass spectrometer in 0.5 s was calculated to be about 8 pg. From the S/N ratio of ~10 as shown in Fig. 2(b) for 100 ng mL^{-1} sample, the LOD of MA may be estimated to be a few pg under the present experimental conditions.

By using the ion source shown in Fig. 1, analyses were made for various real-world samples such as pesticides, plants, soils, liquors, synthetic polymers containing plasticizers, food, *etc.* Each sample gave the characteristic mass spectrum for the vapor ingredients. As an example, the results obtained for the typical insecticide carbaryl (1-naphthylmethylcarbamate, CA, $C_{12}H_{11}NO_2$, MW 201.2) are shown in Fig. 5. The melting point

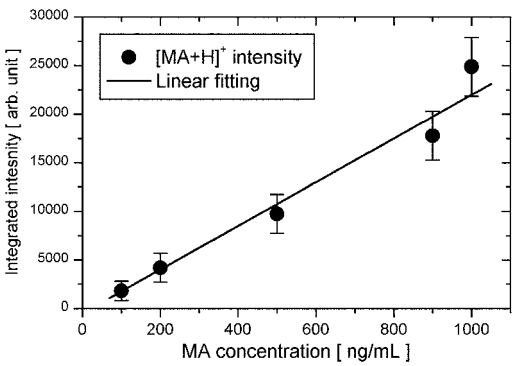

Fig. 4 Calibration curve measured for methamphetamine (MA). Relationship between MA concentration [ng mL^{-1}] and integrated intensities for $[MA + H]^+$ for [aqueous solution of MA of 90 μL + 1 N NaOH(aq) 10 μL]. Sample amount loaded: 100 μL.

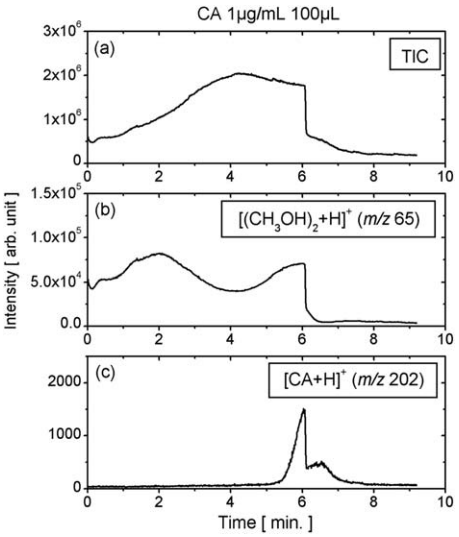

Fig. 5 (a) TIC; (b) and (c) extracted ion chronograms for $[(CH_3OH)_2 + H]^+$ at *m/z* 65 and the protonated carbaryl $[CA + H]^+$ at *m/z* 202 for methanol solution of carbaryl with a concentration of 1 μg mL^{-1}, respectively. 100 μL solution was loaded in a sample vial.

of carbaryl is 142 °C. Its boiling point is difficult to determine, because it decomposes before melting. As the solubility of carbaryl is very low in water, the methanol solution of carbaryl with a concentration of 1 μg mL^{-1} was used as the sample. Fig. 5(a), (b) and (c) show the TIC, extracted ion chronogram of the ions $[(CH_3OH)_2 + H]^+$ at *m/z* 65 and the protonated carbaryl $[CA + H]^+$ at *m/z* 202, respectively. Sudden decreases of TIC, $[(CH_3OH)_2 + H]^+$ and $[CA + H]^+$ signals at about 6 min indicate that the methanol solvent depleted at 6 min after the heaters are turned on. The depletion of 100 μL methanol at 6 min is much faster than the same volume of water (17.5 min in Fig. 2 and 3). The extracted ion chronogram of $[CA + H]^+$ in Fig. 5(c) is quite different from that of $[MA + H]^+$ in Fig. 2. Due to the low volatility of CA, the signal intensity of $[CA + H]^+$ remains at a low level up to ~5 min. Interestingly, it shows a sharp increase at ~5.5 min and decreases sharply after reaching the maximum at ~6 min. The rapid signal increase at the last stage of methanol depletion is worth noting. Just before the complete evaporation, the temperature of the methanol may be close to its boiling point (64.7 °C). The rapid evaporation of methanol molecules from the liquid surface may assist the desorption of dissolved CA. This may be regarded as the solvent vaporization-assisted desorption of less volatile solute near the boiling point of the solvent. This is reminiscent of the events taking place in MALDI where ablation of matrix liberates the analytes to the gas phase. After 6 min, $[CA + H]^+$ shows a small increase followed by a gradual decrease. The rapid evaporation just before the depletion of solvent methanol should be accompanied by the heat consumption from the liquid droplet itself. The local temperature of the sample spot should show the discontinuous increase after the complete evaporation of solvent. This may explain the hump of the signal intensity of $[CA + H]^+$ at ~6.5 min.

As a real-world sample, a piece of basil leaf (5 mm square) was also examined. Protonated camphor ($C_{10}H_{16}O$, MW 152.2) and linalool ($C_{10}H_{18}O$, MW 154.3) were observed as the major ions. The TIC and extracted ion chronograms of $[M + H]^+$ for

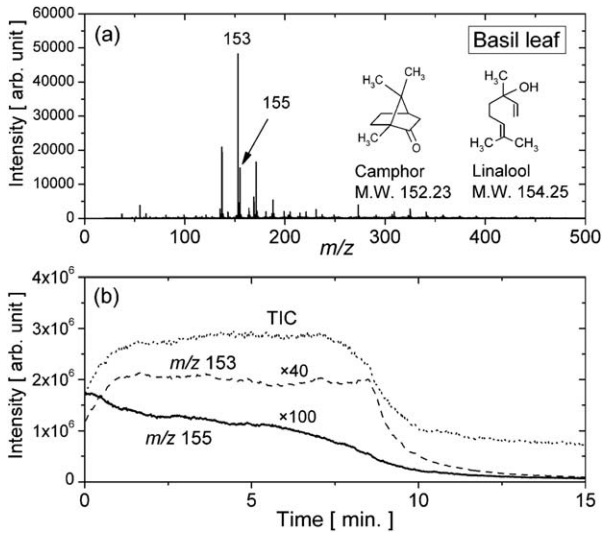

Fig. 6 (a) Mass spectrum for basil leaf measured at 2 min after the heater was turned on; (b) TIC and extracted ion chronograms of $[M + H]^+$ for camphor at *m*/*z* 153 and linalool at *m*/*z* 155 for basil leaf. A piece of basil leaf of about 5 mm square was put into the vial and served for measurement.

camphor and linalool are shown in Fig. 6. The gradual decrease of TIC observed after 7 min suggests that the leaf was being dried during 7–10 min. The discontinuous decrease in $[camphor + H]^+$ (*m*/*z* 153) at 7 min may mean that the evaporation of this component was partly assisted by the evaporation of water in the basil leaf. In contrast, $[linalool + H]^+$ (*m*/*z* 155) showed a rather monotonous decrease with time. It is likely that linalool is more volatile than camphor and its spontaneous evaporation takes place from the basil leaf.

Conclusions

In the DBD ion source developed, the plasma was confined in the double cylindrical dielectric discharge tube. Thus the gaseous analyte molecules introduced through the inner ceramic tube are ionized just outside of the ceramic tube without being exposed to the plasma. This realizes the soft and highly-sensitive ionization for gaseous samples. Methamphetamine could be detected with an LOD of a few picograms. This method is free from contaminants in ambient air because ionization of sample vapor takes place inside the DBD ion source, resulting in the high reproducibility of this method. One drawback is that it takes about 30 min in heating the sample from room temperature to ~150 °C. The sample probe with a much faster temperature programming rate is underway. The conceptual idea of the DBD ion source developed in this work would be applicable as a highly-sensitive and versatile technique to many fields such as safety/security projects, life science, environmental science, agriculture, food industry, *etc*.

Acknowledgements

This work was supported by the Collaborative Development of Innovative Seeds, 'Science & Technology Project for a Safe & Secure Society' from Japan Science and Technology Agency (2007–2008).

References

1 E. C. Horning, M. G. Horning, D. I. Carroll, I. Dizidic and R. N. Stillwell, *Anal. Chem.*, 1973, **45**, 936.
2 R. B. Cody, J. A. Laramee and H. D. Durst, *Anal. Chem.*, 2005, **77**, 2297.
3 H. Chen, J. Zheng, X. Zhang, M. Luo, Z. Wang and X. Qiao, *J. Mass Spectrom.*, 2007, **42**, 1045.
4 N. Na, C. Zhang, M. Zhao, S. Zhang, C. Yang, X. Fang and X. Zhang, *J. Mass Spectrom.*, 2007, **42**, 1079.
5 N. Na, M. Zhao, S. Zhang, C. Yang and X. Zhang, *J. Am. Soc. Mass Spectrom.*, 2007, **18**, 1859.
6 Y. Zhang, X. Ma, S. Zhang, C. Yang, Z. Ouyang and X. Zhang, *Analyst*, 2009, **134**, 176.
7 J. D. Harper, N. A. Charipar, C. C. Mulligan, X. Zhang, R. G. Cooks and Z. Ouyang, *Anal. Chem.*, 2008, **80**, 9097.
8 N. Na, Y. Xia, Z. Zhu, X. Zhang and R. G. Cooks, *Angew. Chem., Int. Ed.*, 2009, **48**, 2017.
9 G. Huang, W. Xu, M. A. Visbal-Onufrak, Z. Ouyang and R. G. Cooks, *Analyst*, 2010, **135**, 705.
10 L. C. Chen, Y. Hashimoto, H. Furuya, K. Takekawa, T. Kubota and K. Hiraoka, *Rapid Commun. Mass Spectrom.*, 2009, **23**, 333.
11 L. C. Chen, H. Suzuki, K. Mori, O. Ariyada and K. Hiraoka, *Chem. Lett.*, 2009, **38**, 520.
12 L. C. Chen, Z. Yu and K. Hiraoka, *Anal. Methods*, 2010, **2**, 897.
13 A. Schütze, J. Y. Jeong, S. E. Babayan, J. Park, G. S. Selwyn and R. F. Hicks, *IEEE Trans. Plasma Sci.*, 1998, **26**, 1685.
14 S. Kanazawa, M. Kogoma, T. Moriwaki and S. Okazaki, *J. Phys. D: Appl. Phys.*, 1988, **21**, 838.
15 K. Hiraoka, H. Furuya, S. Kambara, S. Suzuki, Y. Hashimoto and A. Takamizawa, *Rapid Commun. Mass Spectrom.*, 2006, **20**, 3213.
16 P. E. Siska, *Rev. Mod. Phys.*, 1993, **65**, 337.
17 Y. Ikezoe, S. Matsuoka, M. Takebe and A. Viggiano, *Gas-Phase Ion-Molecule Reaction Rate Constants Through 1986*, Maruzen, Tokyo, 1987.
18 J. H. Gross, *Mass Spectrometry*, Springer-Verlag Berlin Heidelberg, 2004.